Wide field instrument preliminary design for the Wide Field Infra-Red Survey Telescope

David A. Content*[1a], Nerses V. Armani[b], Charles L. Baker[a], Clifton E. Jackson[b], Duncan M. Kahle[a], Jeffrey W. Kruk[a], John P. Lehan[b], Mark E. Melton[a], Eric Mentzell[a], Joseph J. Miko[a], David J. Palace[a], Bert A. Pasquale[a], Hume L. Peabody[a], Brian S. Smith[c], Walter F. Smith[a], Jeffrey W. Stewart[a], David A. Vaughnn[a], Augustyn Waczynski[a], Thomas E. Wallace[a]
[a]NASA Goddard Space Flight Center, Greenbelt MD
[b]SGT, Inc., Greenbelt MD
[c]Stargazer Systems, Annapolis, MD

ABSTRACT

We present the Wide Field Infra-Red Survey Telescope (WFIRST) wide field instrument concept based on the reuse of a 2.4m telescope recently made available to NASA. Two instrument channels are described, a wide field channel (~0.8x0.4degrees, 300Mpix, imaging and spectroscopy over 0.76-2.0um), and an integral field unit (3x3 arcsec, 1Mpix, R{2pixel} ~100 over 0.6-2.0um). For this mission concept, the telescope, instruments, and spacecraft are in a geosynchronous orbit and are designed for serviceability. This instrument can accomplish not only the baseline exoplanet microlensing, dark energy, and infrared surveys for WFIRST, but can perform at higher angular resolution and with deeper observations. This enables significant opportunities for more capable general observer programs. The emphasis on achieving very good imaging stability is maintained from the previous work.

Keywords: WFIRST, Wide Field Imaging, Three Mirror Anastigmat, Telescope

1. INTRODUCTION

The Wide Field Infra-Red Survey Telescope mission has gone through multiple early mission concept studies. This 2010 astrophysics decadal-winning mission concept uses the availability and maturity of large format visible-NIR detector arrays and a wide field of view three mirror anastigmat telescope design to provide an instrument field of view roughly 100x larger than previous imaging cameras such as HST/WFC3 or JWST/NIRCAM. This paper presents the latest concept for the wide field instrument, based on reuse of a 2.4m aperture telescope made available to NASA. A companion paper[1] describes the overall mission concept[2-3], which includes an optional exoplanet imaging coronagraph (see also[4-7]), as well as the Geosynchronous orbit and serviceable spacecraft. We also refer to past point designs for 1.1-1.5m aperture telescope with dedicated 3-5 year missions and related studies[8-13]. The April 2013 report[1] from the WFIRST project jointly with the Science Definition Team (SDT) and the "short form" science report[3] are good references for the enormous astrophysics potential of this mission concept. The project is also studying a potential second instrument, an exoplanet imaging coronagraph[7].

After a brief discussion of requirements, we present the design and capability of this instrument. The instrument for the first time includes an integral field spectrograph in the baseline, as described below.

[1] David.content@nasa.gov; phone 1 301 286-7382

UV/Optical/IR Space Telescopes and Instruments: Innovative Technologies and Concepts VI, edited by Howard A. MacEwen, James B. Breckinridge, Proc. of SPIE Vol. 8860, 88600F
 · doi: 10.1117/12.2025496

2. REQUIREMENTS

The SDT[14] and project were chartered to:
-Develop a design reference mission (DRM) using one of the two 2.4m telescope assets, for 2022 launch; Keep cost comparable to that from predecessor mission studies while achieving all or part of the science priorities for WFIRST.
-Study science potential, rough cost, and risk of adding an optional exoplanet imaging coronagraph instrument.
-Report by April 30, 2013 (Rapid 6 month study time frame)
-Compare science return to DRM1/2 [the previous WFIRST study].
-Include options in the study:
-Mission concept and observatory to be compatible with on-orbit replacement of spacecraft and instrument modules;
-High orbit (Geosynchronous or high earth orbit (HEO))
-Optical communication

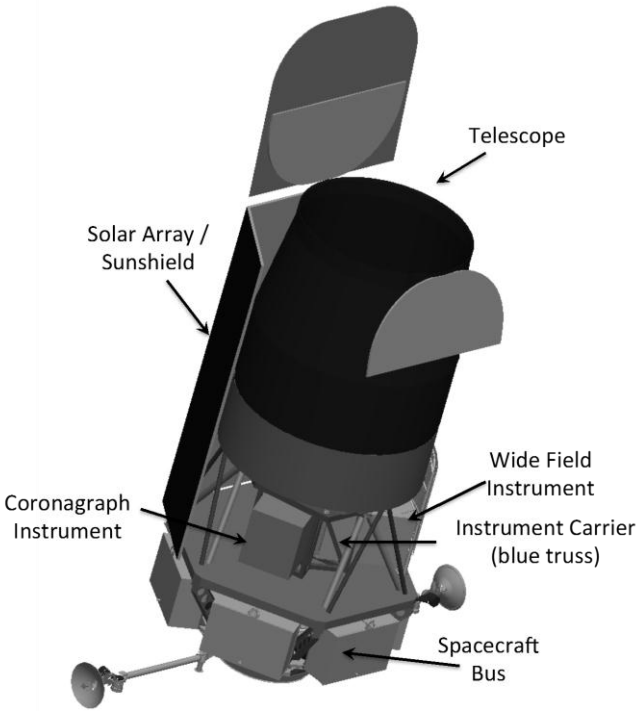

Figure 1: WFIRST-2.4 Observatory configuration featuring the 2.4-m telescope, two modular instruments and a modular spacecraft. bus

Overall instrument requirements initially were conceived to be very similar to those in the predecessor studies. The project and SDT soon realized, however, that the ~3x improvement in collecting area and the 1.8x reduction in point spread function (PSF) core area meant that this observatory could resolve and study fainter objects in less time. The observing strategy was altered to suit this, while still achieving the core programs of exoplanet microlensing, IR surveys, and multiple complementary dark energy measurements.

Figure 1 shows an observatory overview, including the telescope, with its outer barrel and bi-fold doors (one of which is extended for stray light control), fixed solar array/sunshield and spacecraft, and instrument carrier holding the two instruments (described below).

Overall the requirements dictate a large field of regard so that each target and sky survey area can be observed in enough depth and duration (for transient events, particularly the SN 1a and exoplanet microlensing events). The sun angle range of 54-126° is retained from previous work, which allows sufficient time to continuously observe the galactic bulge for up to two seasons per year in order to accomplish the exoplanet microlensing survey. The image quality needed has been taken as a 1.2 micron diffraction limited system (90 nm rms wavefront error), not including small amounts of pointing jitter, for the imaging, with some relaxation possible for the galaxy redshift survey (slitless spectroscopy).

3. TELESCOPE

The telescope consists of a flight design two mirror system, capable (with the additional of a tertiary mirror, here included in the instrument) of forming a three mirror anastigmat design form as appropriate for a wide field of view with good aberration control and a flat final focal surface. The mirrors are light weighted as appropriate for a space system. The secondary mirror is mounted on 6 composite struts, which each can be adjusted for length. This allows alignment compensation on orbit. Further description is in the accompanying mission paper[1]. The telescope is operated at 270K as a preliminary compromise between its range of current thermal qualification temperatures and the desire to limit the near infrared blackbody emission from the telescope to below other backgrounds such as the zodiacal light.

4. WIDE FIELD INSTRUMENT

The wide-field instrument is divided into two modules, a cold instrument module, containing the optics and the focal plane assembly, and the warm electronics module housed on the spacecraft. Optically, the instrument is divided into a wide-field channel, with both imaging and spectroscopy modes, and an integral field unit (IFU) channel. The spectral selection elements, all contained in the single element wheel (filters and galaxy redshift survey grism) are described in Table 1. The key instrument parameters are shown in Table 2. The active field of view (0.28 sq. deg) is not as large as those from the prior (DRM1, DRM2) designs, but the resolution and collecting area are strongly enhanced. They are not quite enhanced by the diameter ratio compared to these designs (1.3, 1.1m unobscured apertures, respectively) because of the central telescope and secondary mirror strut additional small obscuration. We cite a factor of 1.8x reduction in point spread function areal size as the metric of improved resolution; there is also a nearly 3x improvement in collecting area. The grasp (aperture area times field of view area) is significantly higher.

Table 1: Filter and disperser decriptions in the wide field channel element wheel; Wavelengths are in μm. Galaxy redshift survey (GRS) grism dispersion is in arcsec units, $D_\Theta = \lambda/(d\lambda/d\Theta)$, where Θ is sky angle.

Band	Element Name	Min	Max	Center	Width	Dispersion
Element Wheel						
Z	Z087	0.760	0.977	0.869	0.217	4
Y	Y106	0.927	1.192	1.060	0.265	4
J	J129	1.131	1.454	1.293	0.323	4
H	H158	1.380	1.774	1.577	0.394	4
	F184	1.683	2.000	1.842	0.317	5.81
Wide	W149	0.927	2.000	1.485	1.030	1.44
GRS	GRS Grism	1.35	1.95	1.65	0.6	D_Θ= ~150

Figure 2: Field of view comparison, to scale, of the WFIRST-2.4 wide field instrument with wide field instruments on the Hubble and James Webb Space Telescopes. Each square is a 4k x 4k HgCdTe sensor array. The field of view extent is about 0.79 x 0.43 degrees. The pixels are mapped to 0.11 arcseconds on the sky.

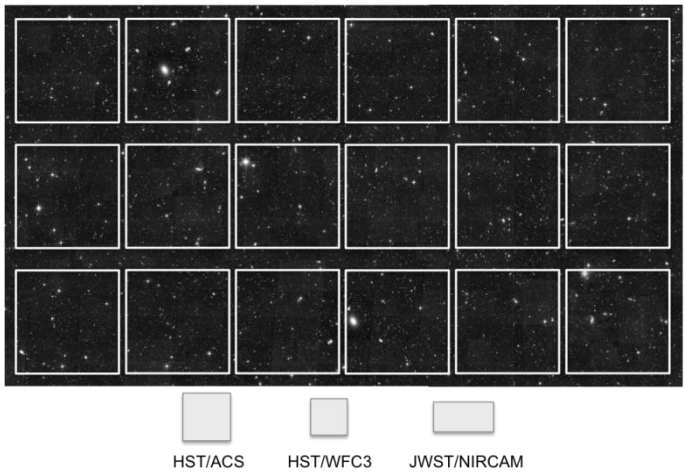

Table 2: Key Instrument parameters for the wide field instrument.

Mode	Wavelength Range (μm)	Sky Coverage (active area)	Pixel Scale (arcsec/pix)	Dispersion	FPA Temperature (K)
Imaging	0.76 – 2.0	0.281 deg^2	0.11	N/A	≤120
GRS Spect.	1.35 – 1.95	0.281 deg^2	0.11	R=550-800 (2-pixel, grism in element wheel)	≤120
SN Ia Spect.	0.6 – 2.0	3.00 x 3.15 arcsec	0.075	R=100 (2-pixel; IFU spectrograph, 1 slice maps to 2 pixels)	≤115
Fine Guiding	0.76 – 2.0	0.281 deg^2	0.11	Guide off wide-field focal plane using windowing function of H4RG	≤120

The instrument module is kinematically mounted to the instrument carrier, which provides the load path between the telescope and the instrument module structure. The instrument module design is similar to the HST/WFC3 design (see Fig. 3) and reuses the design of the WFC3 latches, which can be robotically engaged and disengaged, to mechanically interface instruments to the instrument carrier. The instrument module also includes a grapple fixture to enable its removal by a robotic servicing vehicle. Guide rails on the instrument carrier align the instrument module latches with the instrument carrier latches. Connectors on the instrument module are designed to allow a blind mate to harness in the instrument carrier that runs to the warm instrument electronics module on the spacecraft.

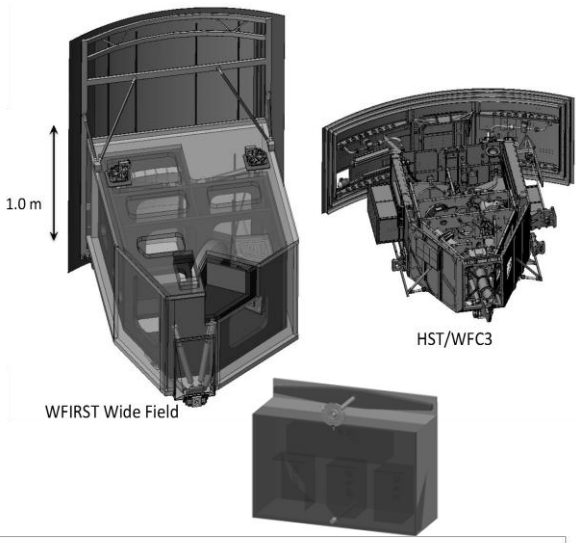

Figure 3: Instrument comparison to HST/WFC3. WFIRST-2.4 wide field is designed to be mechanically similar to the WFC3. Both use composite optical benches, radial latches, passive radiators, and heat pipes for thermal control. Instrument electronics boxes are included among s/c components in two serviceable spacecraft modules.

The instrument module consists of an outer enclosure structure, which is flexured off of the latches and supports the instrument radiators and MLI blankets, and an inner structure, the optical bench, which supports the instrument cold electro-optical components (see Figure 3). The mechanical latches interface directly to the optical bench, via thermally isolating struts, providing a direct load path between the instrument carrier and the alignment-critical optical bench.

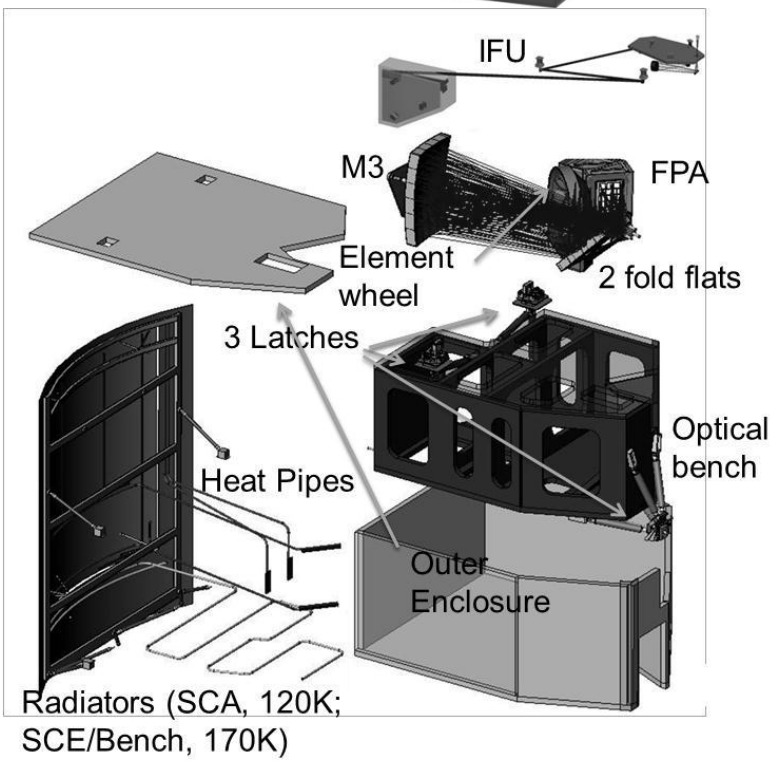

Figure 4: Expanded view of the wide field instrument showing the major elements. The instrument electronics are located in a serviceable spacecraft module. The optical bench and outer enclosure are Al honeycomb panels with composite facesheets. Harnessing is not shown.

4.1 Wide-Field Channel

The wide-field channel optical train consists of a pair of fold flats, a tertiary mirror (M3), a cold pupil mask, an element wheel (EW), and the HgCdTe Focal Plane Array (FPA), see Fig. 4. The FPA uses 18 4k x 4k 10 μm pixel (H4RG) HgCdTe Sensor Chip Assemblies (SCAs), with

a detector wavelength cutoff of 2.1 μm (optical cutoff is limited to 2.0 μm via bandpass filters) and proximate SCA Control Electronics (SCE) boards. The SCAs are arranged in a 6x3 layout with a pixel scale of 0.11 arcseconds/pixel. An 8-position EW provides 6 filters, a dark position (for calibration) and a grism assembly for the GRS. The imaging mode is designed to a diffraction limit of 1.2 μm.

The filters are fused silica substrates with ion-assisted, highly stable bandpass filter coatings with heritage to recent HST instruments. Element bandpasses are listed in Table 2.

The 4-element GRS grism consists of 2 CaF_2 elements and BaF_2 and FK3 correctors. The grism has a spectral range of 1.35-1.95 μm. The equivalent dispersion $D_\Theta=\lambda/(\delta\lambda/\delta\Theta)$, is obtained by multiplying by the angular size of a 2-pixel resolution element. Thus, for a point source resolving power value of R=675, the corresponding value D_Θ is 675*2*0.11= 149 arcsec. A description of the EW complement is shown in Table 1. Figure 5 gives a detailed view of the grism assembly, its spectral dispersion, and its wavefront error over a 3x3 field point grid and its spectral range.

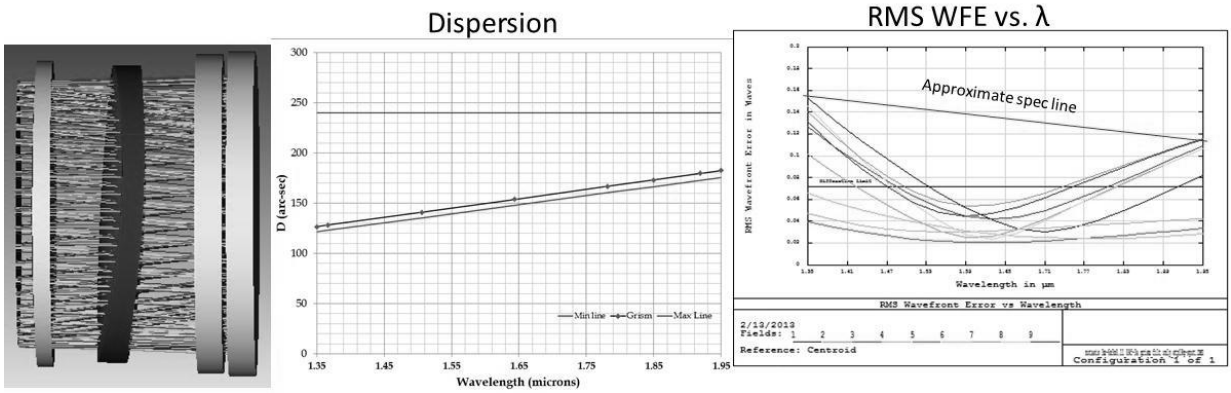

Figure5: CAD model of the GRS grism assembly (left), its spectral dispersion (center), and its rms wavefront error over a 3x3 field point grid and spectral range (right).

4.2 Mechanical structure

The instrument structure, both the outer enclosure and the optical bench, will be made from aluminum honeycomb panels with composite facesheets of cyanate siloxane resin in a carbon fiber matrix. This mature, strong, light, low moisture absorption composite material is a good low thermal expansion match to the ultra low expansion fused silica (ULE®) mirrors used in the instrument. The optical bench structure has top and bottom panels with structural bulkheads between them, and is kinematically supported by and precisely aligned to the instrument carrier at three latch locations via thermally isolating struts. The outer enclosure supports inner and outer MLI blankets that thermally isolate the optical bench from the enclosure and the enclosure from the environment, respectively, two radiators that cool the optical bench and the FPA, the connector blind mate bulkhead, and the instrument servicing grapple.

4.3 Mechanisms

The element wheel is the only mechanism routinely used in science operations. The EW's canted design allows for precise placement of any one of the 6 filters or the grism in a space-constrained volume of the instrument. The wheel assembly includes a cold pupil mask (~100 mm diameter), which blocks the image of the highly emissive struts and obscurations in the telescope pupil to limit parasitic thermal input into the focal plane. The wheel mechanism includes a DC brushless motor with redundant windings that drive a spur and ring gear combination. Motor control is closed loop using a resolver for position feedback.

A second mechanism, which can adjust the second (last) fold flat in pistion, tip, and tilt, is included to compensate for structural changes as the instrument ages and the cold alignment changes. Operation of this adjustment after

commissioning is expected to be on an as needed basis to correct for misalignments due to long term changes, such as moisture outgassing from the composite structural components in the telescope or instrument. The mechanism is secured during launch using a launch lock.

4.4 Thermal design

The wide field channel meets thermal requirements in the GEO orbit by combining a passive, cold-biased thermal design with precise heater control of the critical focal plane hardware. Constant conductance heat pipes are used to transport dissipated and parasitic heat loads to one of two passive radiators. The SCE/bench radiator includes integrated spreader heat pipes to cool the optical bench and SCE mounting plate to ≤170 K. The SCA radiator also includes spreader heat pipes and cools the SCA mosaic plate to ≤120 K. The bottom panel of the optical bench has an embedded ethane heat pipe that transports parasitic loads from the latches, optical aperture, and outer enclosure to the SCE/bench radiator. Two ethane heat pipes connect the SCE mounting plate to the SCE/bench and two methane heat pipes couple the SCA mosaic plate to the SCA radiator.

Proportional-Integral-Derivative (PID) heater control is required to meet SCA and SCE thermal stability requirements (±0.3K over a day, and ±10mK over any 150 sec observation) in the presence of environmental changes (primarily orbital variations in radiator Earth viewing. Three independent (and fully redundant) control zones control the top, middle, and bottom of the SCA mosaic plate, meeting the SCA stability and temperature requirements with margin and maintaining stable gradients across the focal plane (see Fig. 6). A separate, redundant PID controller is used to control one thermal zone on the SCE mounting plate, the SCE thermal variations to no more than ±1 K over any orbit.

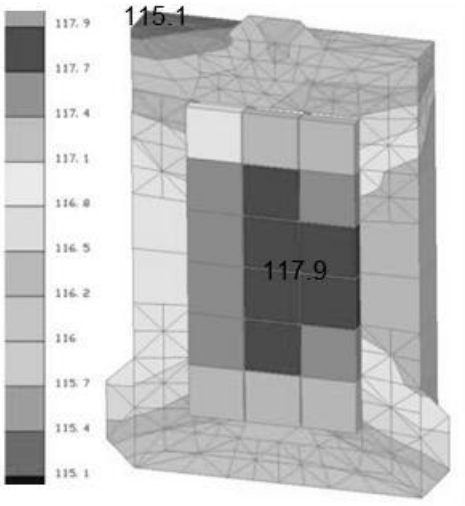

Figure 6: Thermal map of the focal plane assembly, showing small (1K) gradients. This map is stable over several observing seasons and is insensitive to telescope pointing.

4.5 Focal plane assembly

The FPA uses 18 state of the art Hawaii-4 (H4RG) sensor chip assemblies (SCAs) mounted in a 6x3 pattern to a ≤120 K SiC mosaic plate. Each SCA has a 4k x 4k format, 10 μm pixel size. The f/7.9 optical system maps each pixel to 0.11 arcsec square on the sky, providing an FPA active FOV of 0.281 deg^2. Readout wiring limits the extent to which the SCAs can be packed on the mosaic plate, with the minimum spacing in the x (6 SCA) direction being 2.5 mm and in the y (3) direction being 8.546 mm. The FPA (Figure 7) includes a light shield to limit direct illumination to active pixels to control stray light. All 18 SCEs are mounted to a ≤170 K aluminum mounting plate located <12 inches from the SCA mosaic plate. Each SCA is (simultaneously, in sync with all others) read out non-destructively by its SCE in ~5.2s via 32 parallel outputs operating at 100 KHz. One 20 x 20 pixel guide window is also read out in sync at 20 Hz from each SCA (position in each SCA variable, depending on guide star location). All SCA-harness-SCE units are identical, simplifying production and sparing. The entire assembly is surrounded, except for the incoming optical beam, by a combined radiation and stray light shield enclosure. The shield extends around the second fold flat (F2) and is primarily designed to minimize the exposure of the SCAs and SCEs to the trapped electron environment in geosynchronous orbit.

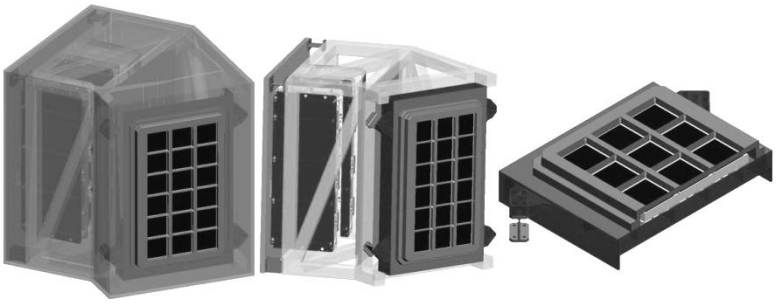

Figure 7: Focal plane assembly; Left panel: entire assembly including SCAs (dark squares), light shield, and radiation shield. Middle panel: view with radiation shield removed, showing composite structure, SCE cards, and thermal standoffs. Right panel: cutaway view of SCA mosaic and SCA carriers.

4.6 Wide Field Electronics and Wide Field Channel Signal Flow

The wide field instrument electronics (handling both the wide field and IFU channels) are summarized (including redundancy) in the Figure 8 electronics block diagram. Five warm electronics boxes (Instrument Command and Data Handling box, or ICDH (prime and redundant with only one operational), Mechanisms Control Box, or MCB, and two Focal Plane Electronics, or FPE, boxes) are mounted to the serviceable instrument warm electronics module provided by the spacecraft, with interconnects to the cold instrument module being made via "blind mate" connections provided for both modules to harness permanently mounted to the spacecraft and the instrument carrier. ICDH functions are noted in detail in the block diagram, with key areas being the lossless data compression of the 19 science image data streams and their multiplexing for delivery to the spacecraft, the provision of the SCA and SCE thermal control loops, and the processing of the SCA guide window sub-images. The MCB controls the EW to select filter/grism positions on a routine basis. The signal flow off the focal plane is controlled by the cold SCEs mounted in the FPA and the warm SCE Control Unit (SCU) boards mounted in the FPE boxes on the spacecraft (one dedicated SCE/SCU chain for every SCA, all processing data in parallel). During an integration, image frames interleaved with guide window data are delivered to an SCU for processing every ~5.2 s. The guide window data is stripped out and sent to the ICDH for processing. The image frame data is handled two ways: averages of groups of four frames are passed to the ICDH for downlink, and Sample-Up-The-Ramp (SUTR)[15] processing is applied to all readouts. A table of cosmic-ray hits and pixel saturation data (count rate prior to saturation) is passed to the ICDH for downlink at the end of each exposure. This table adds only a few percent to the total data volume, but the availability of corrections at the full 5.2 second readout cadence mitigates the more frequent incidence of radiation events in the geosynchronous orbit (compared to the Sun-Earth L2 orbit of prior WIRST studies) and maximizes the signal-to-noise that can be obtained in ground processing of the "multi-accum" style raw data. The ICDH applies lossless compression and multiplexes the 18 parallel data streams for transmission to the spacecraft. Preliminary studies indicate that compression factors greater than two can be achieved; a factor of 2 has been assumed in the data volume estimates.

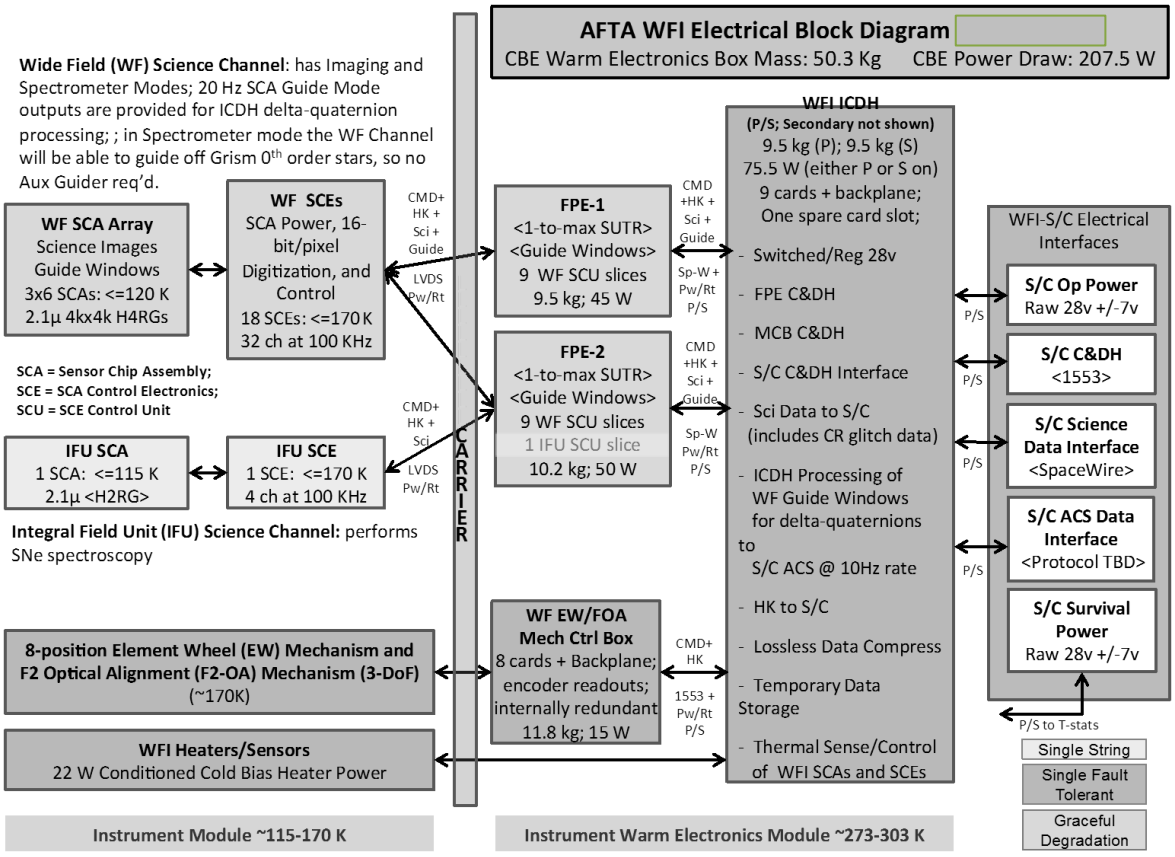

Figure 8: Electronics block diagram for the wide-field instrument.

4.7 Integral Field Unit

The integral field unit is a separate instrument channel contained within the wide-field instrument. It uses a small field of view (3.00 x 3.15 arcsec) aperture to limit the sky background entering the instrument channel. An optical relay reimages this small field onto an image slicer and spectrograph covering the 0.6-2.0 μm spectral range (see Figure), resulting in a detector format wherein 21 slices, 3.0 x 0.15 arcsec each (see Figure 9), are imaged onto separate pixel sections of an 18 μm detector (H2RG, 2048 x 2048 x 18 μm). The slicer is based on the commercially available reflective image slicer from WinLight, a version of which has been through space environmental testing. While there are a substantial number of elements, they are small (a maximum 5 cm) and work in a slow optical beam with relaxed stability tolerances. Figure 10 shows the slicer and spectrograph layout; Figure 4 above shows how the entire IFU optical train is packaged into the instrument.

The pixel scale at the focal plane is 0.075 arcsec. The resolving power is flattened by the use of a compound prism of materials Infrasil and SF11 to a typical value of 100 (2 pixels), see Fig. 11.

The slicer and spectrograph elements are packaged in a separate optical bench that is installed into the wide-field instrument housing. The opto-mechanical assembly is held at the same instrument temperature (170 K) as the rest of the wide-field instrument. The focal plane assembly includes a cryogenic heat pipe to maintain a temperature of 115 K at the focal plane and provide good thermal stability, so as to control the dark current and read noise that limits the signal to noise ratio at each end of the spectral range.

While primarily designed around the need to observe high redshift type IA SNe, this observing mode would be of use in a general observer program, to observe objects of interest, as the data product is a data cube ($image_x$, $image_y$, spectral position) with good stability and high S/N ratio.

This configuration achieves rapid deep spectroscopy on one object at a time; prior point designs used a slitless spectroscopy mode in the wide field channel to obtain similar data. However, the speed advantage increases strongly with the telescope diameter. In this case the SN1a observations can be made more quickly using the IFU approach. In addition, this capability of quickly obtaining background-limited observations on single object is likely to also be useful for GO and observations of transient objects.

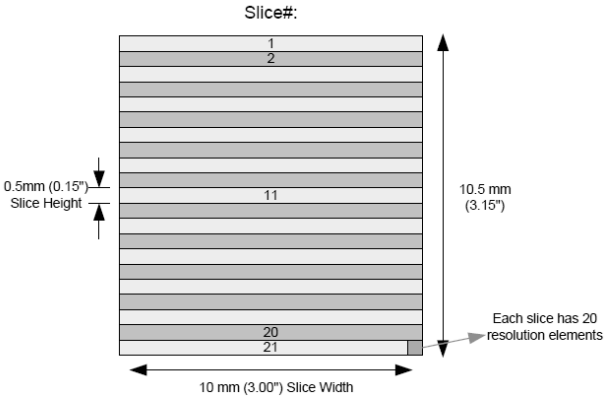

Figure 9: The image slicer has 21 mirrors, 0.5 mm wide, each 0.15 arcsec field wide.

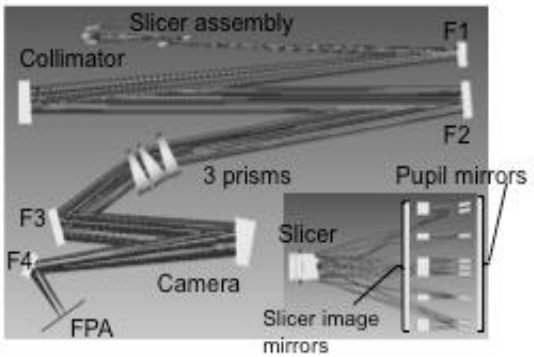

Figure 10: Layout of the slicer assembly (inset) and spectrograph modules of the IFU. The relay is not shown.

4.8 Stability

The telescope and wide field instrument are made from low coefficient of thermal expansion materials such as graphite composite and ultra low expansion fused silica. These composites can be engineered for both low moisture uptake and rapid degassing of the small amount of water absorbed; in any case little outgassing occurs after the telescope goes below 273K (0 C). The fixed sunshade/solar array shadows the payload for all targets within the field of regard. The principal thermal changes are driven by slight sun angle variations and small amounts of thermal backloading from the earth for an observatory in geosynchronous orbit. Overall stability should be enhanced by large factors relative to that of the Hubble space telescope in low orbit.

5. SUMMARY

We have described the WFIRST-2.4 wide field instrument early concept design. Relative to prior designs it is more sensitive, with a finer resolution, similar field area, and higher collecting area. It can accomplish the WFIRST science laid out in the Decadal with time remaining for general observer observations in a five year mission.

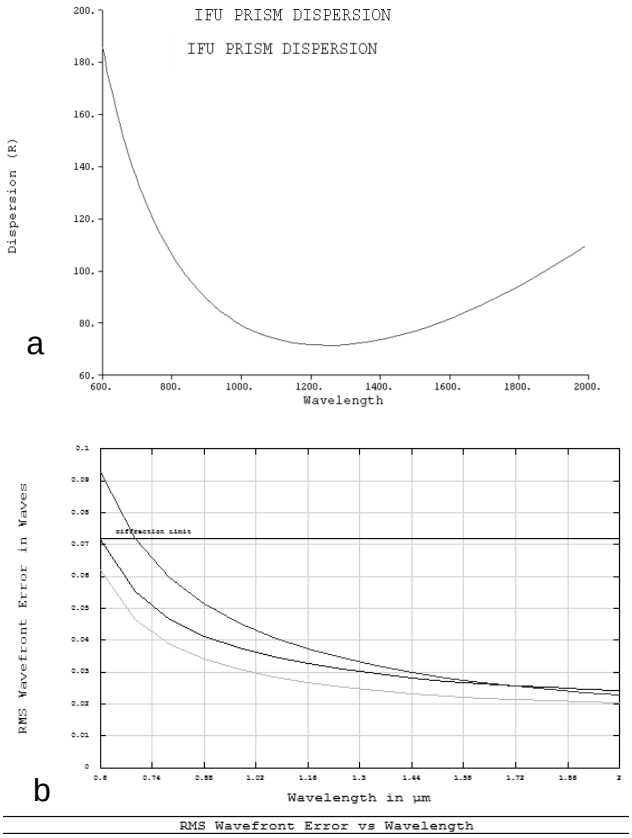

Figure 11: The variation in resolving power of the IFU over the bandpass is shown in a. The diffraction limited imaging performance of an edge slice (center slices are better) at 3 field points (center, halfway out, and nearly at an edge of the slice, is shown in b.

ACKNOWLEDGEMENTS

This work is adapted, with slight updates, from the April 2013 final report jointly written by the SDT and WFIRST project team. We gratefully acknowledge that any work such as this is a product of the combined efforts of a large team. Particularly we want to thank the current WFIRST SDT, and project support staff. This work was funded by NASA.

REFERENCES

[1] Content, D., Aaron, K. M., Alplanalp, L., Anderson, K., Capps, R., et al., "Wide Field Infra-Red Survey Telescope (WFIRST) 2.4-meter Mission Study," Proc. SPIE 8860 {this volume}.
[2] Spergel, D., Gehrels, N., Breckinridge, J., Donahue, M., Dressler, A., et al., "Wide-Field InfraRed Survey Telescope-Astrophysics Focused Telescope Assets WFIRST-AFTA Final Report," arXiv:1305.5422v2 [astro-ph.IM].
[3] Weinberg, D., Gehrels, N., Breckinridge, J., Donahue, M., Dressler, A., et al., "WFIRST-2.4: What Every Astronomer Should Know," arXiv:1305.5425[astro-ph.IM].
[4] Krist, J. E., Shaklan, S., Moody, D., "End-to-end optical modeling of potential coronagraphs for the AFTA space telescope,", Proc. SPIE 8864-64 (2013).
[5] Carlotti, A., Kasdin, N. J., Vanderbei, R. J., "Shaped pupil coronagraphy with the AFTA telescope," Proc. SPIE 8864-34 (2013).
[6] Groff, T. D., Kasdin, N. J., Pueyo, L. A., Shaklan S., "Wavefront control scenarios for a coronagraph on the AFTA space telescope," Proc. SPIE 8864-37 (2013).
[7] Shaklan, S., Foote, M. C., Levine, M., Rodgers, J. M., Underhill, M., et al., "Coronagraph design for the AFTA telescope," Proc. SPIE 8864-39 (2013).
[8] Green, J., et al., "Wide-Field InfraRed Survey Telescope (WFIRST) Final Report", arXiv 1208.4012 (2012).

[9] Content, D. A., Dittman, M. G., Firth, B., Howard, J. M., Jackson, C. E., et al., "Joint Dark Energy Mission optical design studies", Proc. SPIE 7731, 77311D (2010); doi:10.1117/12.859144.
[10] Jurling, A. S., Content, D. A, "Wavefront sensing for WFIRST with a linear optical model," *Proc. SPIE*. 8442, 844210 (2012); doi:10.1117/12.925089
[11] Goullioud, R., Content, D. A., Kuan, G. M., Moore, J. D., Chang, Z., et al., "Wide Field Infrared Survey Telescope [WFIRST]: telescope design and simulated performance," *Proc. SPIE*. 8442, 84421U; doi:10.1117/12.927808.
[12] Content, D. A., Goullioud, R., Lehan, J. P., and Mentzell, J. E., "Optical design trade study for the Wide Field Infrared Survey Telescope [WFIRST]," Proc. SPIE 8146, 81460Y (2011); doi:10.1117/12.898528.
[13] Content, D. A., Dittman, M. G., Firth, B., Howard, J. M., Jackson, C. E., et al., "Joint Dark Energy Mission optical design studies," Proc. SPIE 7731, 77311D (2010); doi:10.1117/12.859144.
[14] Science Definition team, listed at http://wfirst.gsfc.nasa.gov/science/sdt_public/sdt_membership.html.
[15] Offenberg, J.D.; Fixsen, D.J.; Mather, J.C., "Memory-Efficient Up-the-Ramp Processing with Cosmic-Ray Rejection", PASP, **117**, 94 (2005).